A spatially explicit analysis to extrapolate carbon fluxes in upland tundra where permafrost is thawing

HANNA LEE*[1], EDWARD A. G. SCHUUR*, JASON G. VOGEL†, MARTIN LAVOIE*, DHIMAN BHADRA‡ and CHRISTINA L. STAUDHAMMER§[2]

*Department of Biology, University of Florida, Gainesville, FL 32611, USA, †Department of Ecosystem Science & Management, Texas A & M University, College Station, TX 77843, USA, ‡Department of Statistics, University of Florida, Gainesville, FL 32611, USA, §School of Forest Resources and Conservation, University of Florida, Gainesville, FL 32611, USA

Abstract

One of the most important changes in high-latitude ecosystems in response to climatic warming may be the thawing of permafrost soil. In upland tundra, the thawing of ice-rich permafrost can create localized surface subsidence called thermokarst, which may change the soil environment and influence ecosystem carbon release and uptake. We established an intermediate scale (a scale in between point chamber measurements and eddy covariance footprint) ecosystem carbon flux study in Alaskan tundra where permafrost thaw and thermokarst development had been occurring for several decades. The main goal of our study was to examine how dynamic ecosystem carbon fluxes [gross primary production (GPP), ecosystem respiration (R_{eco}), and net ecosystem exchange (NEE)] relate to ecosystem variables that incorporate the structural and edaphic changes that co-occur with permafrost thaw and thermokarst development. We then examined how these measured ecosystem carbon fluxes responded to upscaling. For both spatially extensive measurements made intermittently during the peak growing season and intensive measurements made over the entire growing season, ecosystem variables including degree of surface subsidence, thaw depth, and aboveground biomass were selected in a mixed model selection procedure as the 'best' predictors of GPP, R_{eco}, and NEE. Variables left out of the model (often as a result of autocorrelation) included soil temperature, moisture, and normalized difference vegetation index. These results suggest that the structural changes (surface subsidence, thaw depth, aboveground biomass) that integrate multiple effects of permafrost thaw can be useful components of models used to estimate ecosystem carbon exchange across thermokarst affected landscapes.

Keywords: ecosystem c balance, microtopography, scaling, semivariogram, thermokarst

Received 12 May 2010 and accepted 18 June 2010

Introduction

Climate change has led to an increase in mean annual air temperature on a global scale (ACIA, 2005). Among terrestrial ecosystems, high-latitude ecosystems (boreal forest and tundra) have undergone the most drastic changes over the last 100 years (Overpeck et al., 1997; Serreze et al., 2000); the increase in temperature has been nearly three times greater than the global mean (IPCC, 2007). The temperature increase in high-latitude ecosystems has contributed to thawing of permafrost (ground that is frozen for more than 2 consecutive years) (Osterkamp & Romanovsky, 1999; Hinzman et al., 2005). In upland tundra, thawing of ice-rich

permafrost can create localized surface subsidence called thermokarst (Davis, 2001; Jorgenson et al., 2006). This results in permanent land surface subsidence (Schuur et al., 2008) due to the draining of water that formerly upheld the ground in the form of ice-wedges. The scale and magnitude of thermokarst affects local hydrology (Jorgenson et al., 2006) and may bring greater changes in soil properties such as increased temperature, moisture, and nutrient availability than increased degree of permafrost thaw alone.

Permafrost is distributed over 14% of the global land surface and stores more than 50% of terrestrial carbon (C, 1672 Pg of soil C, $1 Pg = 1 \times 10^{15}$ g) as soil organic matter (Schuur et al., 2008; Tarnocai et al., 2009). The frozen conditions of permafrost slow down decomposition of annual plant litter inputs, storing them as new soil organic matter every year. Thawing of permafrost and thermokarst development may stimulate organic matter decomposition as a result of altered soil properties, and increased rates of decomposition may in turn exacerbate global scale warming. Some researchers

[1]Present address: H. Lee, Department of Biology, New Mexico State University, Las Cruces, NM 88003, USA.

[2]Present address: C. L. Staudhammer, Department of Biological Sciences, University of Alabama, Tuscaloosa, AL 35487, USA.

Correspondence: H. Lee, tel. + 1 575 646 2934, fax + 1 575 646 5665, e-mail: hlee@nmsu.edu

have observed increased net ecosystem exchange of CO_2 (NEE) from high-latitude ecosystems as a result of increased air and soil temperature, releasing more carbon to the atmosphere as greenhouse gases (Chapin *et al.*, 2000; Oechel *et al.*, 2000), whereas others have found that increased soil moisture and temperature are directly responsible for increased NEE (Oberbauer *et al.*, 1992). Indirectly, increased temperature in permafrost soil may stimulate soil organic matter decomposition and release nutrients into the soil, which in turn positively feeds back to faster decomposition of soil organic matter (Mack *et al.*, 2004).

Alternatively, changes in soil properties caused by permafrost thaw and thermokarst development may stimulate carbon uptake by increased primary production in the permafrost zone. Previous studies have observed the effects of climate change on carbon uptake in high-latitude ecosystems including increased primary production (Schuur *et al.*, 2007) and expansion and enlargement of shrubs and invasion of trees in tundra (Macdonald *et al.*, 1993; Sturm *et al.*, 2005). This has the potential to offset, in part, carbon loss from soil organic matter decomposition. Therefore, changes in tundra carbon release and uptake as a result of permafrost thaw and thermokarst development will vary based on the processes that stimulate decomposition (i.e. soil temperature and moisture availability) and those that stimulate aboveground primary production via increased nutrient availability (Shaver *et al.*, 2000, 2001).

In an upland tundra ecosystem, the progression of permafrost thaw and thermokarst development over several decades in the landscape has led to increases in primary production and changes in plant species composition from tussock forming sedge species to shrub species (Schuur *et al.*, 2007). At the initial stage of permafrost thaw and thermokarst development, the ecosystem was a net carbon sink because of increased primary production (Vogel *et al.*, 2009). However, at the later stage of thaw, the ecosystem was a net carbon source because of increased ecosystem carbon emissions, particularly from decomposition of old carbon stored in the deeper permafrost layer (Schuur *et al.*, 2009). These patterns in ecosystem carbon emissions and uptake corresponded to permafrost thaw and thermokarst terrain that had developed approximately 50 or more years.

The changes in ground topography as a result of thermokarst driven subsidence has resulted in a complex microtopography (MT) where subsided areas collect water and can become water saturated, while relatively elevated areas become drier within the same site. Our previous observations indicated that the microsites (patches of surface subsidence) had higher soil temperature, higher soil moisture, and more shrub growth (Lee *et al.*, 2007). Supporting these observations, we observed greater belowground CO_2 production in areas with increased permafrost thaw and surface subsidence, likely as a result of increased rate of soil organic matter decomposition (Lee *et al.*, 2010). These results indicated that ecosystem variables such as soil temperature, aboveground plant biomass, and degree of ground subsidence could be used as proxy variables for ecosystem carbon fluxes in sites with thawing permafrost and thermokarst development.

Measurements from Schuur *et al.* (2009) and Vogel *et al.* (2009) were well replicated over time, but those measurements were taken at relatively few points distributed throughout the study area. Intensive sampling at a point scale over time describes the large temporal variability (i.e. diurnal carbon cycles and seasonal carbon cycles) quite well, while eddy covariance tower measurements integrate one, much larger area than those taken from a point scale. However, thermokarst terrain is composed of discrete and localized landscape features that form through time and then persist on the landscape, acting as independent units in that most ecosystem measurements taken 5–15 m apart show no sign of similarity (Lee *et al.*, 2007). Several studies have shown that carbon flux in tundra is highly variable throughout the day and year (Heikkinen *et al.*, 2002; Kwon *et al.*, 2006). Additionally, aboveground biomass and NDVI may also be highly variable year to year in tundra ecosystems (Boelman *et al.*, 2005), which in turn may be related to high variability in tundra ecosystem gas exchange (Boelman *et al.*, 2003). A multiscale observational study suggested that due to the spatial heterogeneity in arctic systems, it is important to determine the relationships between measurements taken at fine scales and at coarser scales especially for leaf area index (Williams *et al.*, 2008). Thermokarst terrain varies substantially in vegetation, thaw depth (TD), and drainage characteristics. These characteristics suggest that a study design may need to incorporate many point measurements across a relatively large area to understand how permafrost thaw and thermokarst, in particular, affects landscape scale carbon balance (i.e. hundreds of meter square area). Intensive temporal measurements at this 'intermediate scale' would take a prohibitive amount of time and resources. Therefore, correlations between relatively simple ecosystem variables and carbon flux would be useful for determining carbon flux from a larger area.

Upscaling is an extrapolating process that uses a point scale and/or site-specific scale measurements to predict ecosystem or earth system processes (Harvey, 2000). In terrestrial systems, many processes are spatially heterogeneous and non-linear. Because of this,

it is important to recognize spatial patterns when predicting ecosystem processes to minimize introduction of significant errors imposed by spatial heterogeneity in terrestrial systems. We were interested in characterizing spatial heterogeneity of ecosystem properties and ecosystem carbon fluxes in tundra landscape created by permafrost thaw and thermokarst development using geostatistical analysis to assist in upscaling of ecosystem measurements. We used a mixed model procedure that included both independent variables known to generally correlate with ecosystem carbon dynamics in the arctic [i.e. soil temperature, moisture, vegetation biomass, normalized difference vegetation index (NDVI)] in combination with variables that are unique to locations with permafrost thaw (i.e. surface subsidence and TD). In addition, we examined the spatial structure of the explanatory variables for potential use in upscaling of ecosystem carbon balance under scenarios such as permafrost thaw and thermokarst development from northern regions.

Materials and methods

Site description

This study was conducted in upland tundra near Healy, Alaska, just outside of Denali National Park [Eight Mile Lake (hereafter 'EML gradient sites'): 63°52′42″N, 149°15′12″W; Schuur et al., 2009]. At this site, ground temperature and deep permafrost temperatures to depths of 30 m have been monitored since 1985 (Osterkamp & Romanovsky, 1999). Ground subsidence as a result of permafrost thaw and thermokarst development has also been observed within the landscape (Osterkamp et al., 2009). The area is a gentle north-facing slope ($<5°$) with discharge water draining into the adjacent EML. The organic horizon, 0.45–0.65 m thick, covers cryoturbated mineral soil that is a mixture of glacial till (small stones and cobbles) and windblown loess. Permafrost was found within one meter of the soil surface, classifying these soils in the order Gelisol.

Three sites were established in 2003 based on the degree of permafrost thaw and resulting ground subsidence (Schuur et al., 2007): the Minimal Thaw site is the least disturbed of the three sites and is a typical moist acidic tussock tundra site scarcely covered by dwarf shrub sub-layer dominated by tussock forming sedges (Eriophorum vaginatun and Carex spp.) and an understory of mosses and lichens, with little ground subsidence. The Moderate Thaw site is located adjacent to the permafrost monitoring borehole (Osterkamp & Romanovsky, 1999), where patchy areas of ground subsidence have started to occur. The vegetation composition of the Moderate Thaw site was similar to the Minimal Thaw site, but with increased biomass of all plant groups. The Extensive Thaw site contains large-scale ground subsidence and shrubs such as blueberry (Vaccinium uliginosum) and cloudberry (Rubus chamaemorus), that have become the dominant vegetation at the expense of tussock-forming sedges (Schuur et al., 2007).

Soil organic pools to a depth of 1 m averaged $59.8 \pm 2.8 \, kg \, C \, m^{-2}$ across all three sites (Schuur et al., 2009). The ratio of carbon to nitrogen (C:N) in surface 5–15 cm soils ranged from 33.4 to 57.6 across all three sites, and the C:N at the three sites were not statistically different (H. Lee, unpublished results, 2009). The mean active layer measured from 2004 to 2006 at the Extensive Thaw site ($78.3 \pm 4.5 \, cm$) was greater than that of the Minimal Thaw ($68.7 \pm 2.0 \, cm$), with Moderate Thaw ($70.0 \pm 2.0 \, cm$) being the intermediate, but not significantly different from the other sites (Vogel et al., 2009). These different moisture conditions often covary with soil temperature, microsite differences in plant community composition, and increased active layer thickness (ALT), with more saturated areas having deeper TD.

Land surface survey

As a preliminary study, we surveyed the landscape to quantify surface subsidence created by permafrost thaw and thermokarst at the three EML gradient sites in 2004. Fine scale ground subsidence was estimated using Theodolite Total Station surveying equipment (Leica TPS400, Leica Geosystems, St Gallen, Switzerland). Transects were established within a 50 m × 50 m area at each site (Minimal Thaw: 15, Moderate Thaw: 11, Extensive Thaw: 10) and 600 ± 50 points were surveyed within each site. Sampling points along a single transect were not equally spaced, but were approximately 50 cm apart. Tussocks were avoided to minimize variations in surface topography not directly due to thermokarst; all topography measurements represent the moss/soil surface. The x, y, z (longitude, latitude, altitude) coordinates were then normalized for hillslope trends along the z-axis to minimize the effect of hillslope. From this, we excluded the top 5% of the z-axis measurements as outliers and obtained means of the remaining highest 10% of the points per site. All of the z-axis values were normalized according to the mean of the highest 10% of the values as a measure of surface subsidence created as a result of thermokarst. This procedure (hillslope detrending) was done separately for each site. Therefore, the surfaces with lower relative elevation largely represent surface subsidence created by permafrost thaw and thermokarst, whereas the surfaces with higher relative elevation represent elevated surfaces that did not subside (Schuur et al., 2009). This relative elevation measurement representing surface subsidence created by permafrost thaw and thermokarst development will be referred to as 'MT' throughout this study.

Measurement grid establishment

In 2006, a subset of the surveyed area was established as measurement grid points at each EML gradient site (Fig. 1) to quantify ecosystem variables such as soil temperature, moisture, TD, and aboveground biomass as well as ecosystem CO_2 fluxes [gross primary production (GPP), ecosystem respiration (R_{eco}), and net ecosystem exchange (NEE)], and to relate these measurements to MT. These measurements encompassed an equally spaced 5 m grid within a 50 m × 25 m
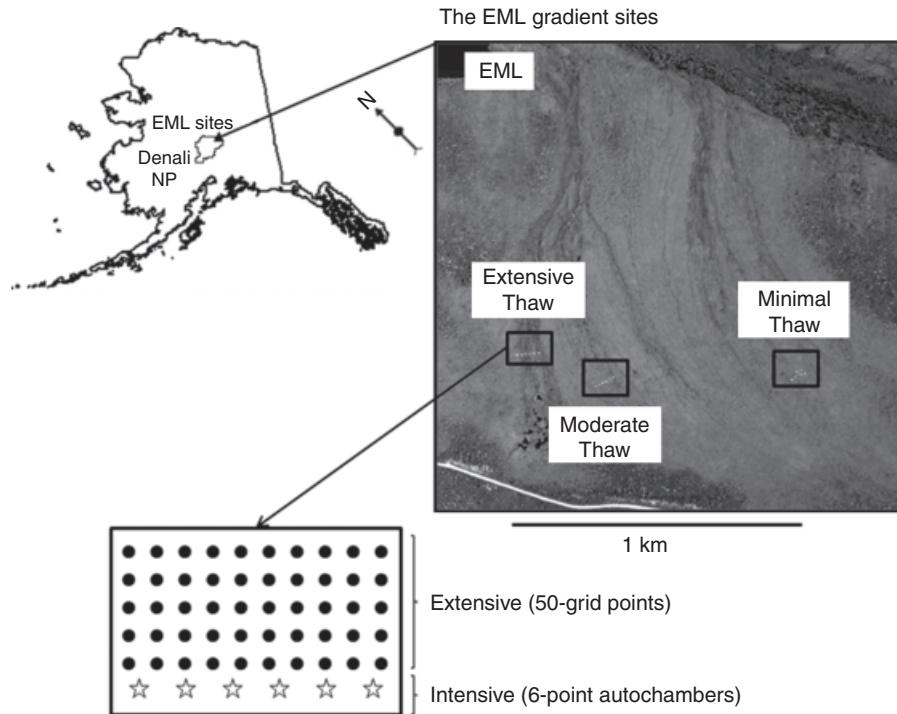
The EML gradient sites

Fig. 1 The Eight Mile Lake (EML) gradient sites and the sampling diagram showing extensive (50 grid points equally distributed in 5 m) and intensive measurements (six points for autochamber measurements). The dark spot on the upper left corner is EML, white line on the bottom is a road, gray areas are tundra vegetation, and dark gray lines where Extensive and Moderate Thaw sites are established are subsided land surface created as a result of permafrost thaw and thermokarst development. The white dots within each site are chamber collars of intensive measurements.

area, so that there were 50 sampling points per Minimal, Moderate, and Extensive Thaw site (hereafter '50 grid points').

We used differential global positioning systems (GPS) to determine the location and topographical surface features of the 50 grid points at the EML gradient sites. We were also interested in fine scale topographical features, since the differential GPS method provides precision up to 1 vertical centimeter (Little *et al.*, 2003). One GPS unit (Trimble 5400) was installed at a nearby USGS marker (WGS84, 63°53′16.56″N, 149°14′17.92″W) and the other GPS unit was used to measure the coordinates of interest. Measurements were corrected relative to the marker to obtain better accuracy. The longitude and latitude information collected from the differential GPS and the Theodolite Total Station was converted to the Universal Transverse Mercator (UTM) coordinate system using ArcGIS 9.3.

Soil properties

Soil temperature sensors were deployed in a manner that captured the spatial variability in soil temperature at the 50 grid points within the EML gradient sites. IButton Thermochron temperature loggers (Maxim Inc., Dallas, TX, USA) were buried at each grid point to a depth of 10 cm and temperature was logged for 3 days in continuous 30 min intervals. Mean soil temperatures at 10 cm depth were obtained for the 3 days

of measurements and normalized within a measurement period. Higher soil temperature estimated from this normalization indicated that soil temperature at a particular microsite was higher than the mean of the 50 grid points. These observations were used to describe spatial variability of soil temperature.

Soil TD was measured during the peak of the growing season (mid-July) in 2006 and 2007 at each of the 50 grid points. Depth from the surface was recorded using a 1/16″ rod that was pushed into the ground until it hit the frozen layer. Soil moisture content was measured by volumetric water content (VWC) using a Campbell Scientific CS616 water content reflectometer and a hand-held voltmeter at 10 cm depths in the soil at each of the 50 grid points. The water content reflectometer was inserted in soil vertically, thus integrating near surface soil temperatures of 0–10 cm depth. However, we calibrated the CS616 specifically for the EML gradient sites at nearby points using direct sampling of soil water content made with destructive soil sampling to compare with CS616 values made at those same nearby points (Lee *et al.*, 2010).

Aboveground biomass and vegetation index

Aboveground plant biomass was estimated for the 50 grid points within the EML gradient sites during the most productive time of the year (mid-July to early-August) in 2006 using

the point-framing method. The point-framing method quantifies aboveground plant biomass as well as species composition. We used the same method presented in Schuur *et al.* (2007) and used allometric equations developed for the EML gradient sites to estimate total aboveground biomass ($g\,m^{-2}$) of a small quadrat ($40\,cm \times 40\,cm$) used in the point-framing method. In this measurement, we only accounted for the fresh vegetation productivity in that year, excluding dead biomass.

We indirectly assessed vegetation biomass at the 50 grid points using the NDVI, which was measured at the same time aboveground biomass was estimated using the point-framing method. The NDVI is an estimate of greenness and leaf area, whereas the point-framing method is an indirect estimate of total aboveground biomass including green leaves and stems. The NDVI is estimated by the differences between near infrared radiation (NIR) and visible wavelength (VIS) [NDVI = (-NIR–VIS)/(NIR + VIS)]. We used a hand-held ADC camera (Tetracam Inc., Chatsworth, CA, USA) to take photographs of the vegetation encountered in point-framing and later used TETRACAM PIXEL WRENCH2 software (Tetracam Inc., Chatsworth, CA, USA) to process the images to estimate NDVI.

Ecosystem carbon fluxes

Ecosystem CO_2 fluxes were measured to estimate R_{eco}, GPP, and NEE at the 50 grid points within the EML gradient sites. NEE was estimated from measurements of CO_2 fluxes under ambient light and absolute dark [$NEE_{light} = GPP - R_{eco}$; $NEE_{dark} = (-)\,R_{eco}$]. We used a closed static chamber system to measure CO_2 flux using an infra-red gas analyzer (Li-820, LI-COR Biosciences, Lincoln, NE, USA), as air circulated through attached to a $40\,cm \times 40\,cm \times 40\,cm$ clear acrylic chamber. Typically, these chamber measurements are made via setting the chamber on a collar top, but we used a windshield skirt around the chamber to prevent wind-air mixing during the flux measurements. These flux measurements were compared with flux measurements taken from automated chamber system at the same sites to validate the use of windshield skirt because it was not sealed in tundra; our CO_2 flux measurements fell within the range of flux measured from automated chamber system at the same time frame. The flow of air was maintained at $1.5\,L\,min^{-1}$. We scrubbed out moisture going into the infra-red gas analyzer using $MgClO_4$ from the tubing before measuring CO_2 fluxes. Therefore, we did not use any moisture conversion in our flux calculations. Light intensity was measured as photosynthetically active radiation (PAR, $\mu mol\,m^{-2}\,s^{-1}$) using a LICOR quantum sensor placed inside the chamber. To take the dark CO_2 flux measurement, we blocked the light by covering the chamber with a reflective cloth designed to fit the chamber exactly. We used a hyperbolic equation to describe the relationships between PAR and growing season GPP and NEE (Thorney & Johnson, 1990). Only first 90 s of CO_2 concentrations were taken for the calculations of CO_2 fluxes. For R_{eco}, we used the exponential relationship developed by Bubier *et al.* (2003), which was adjusted by Vogel *et al.* (2009) for the EML gradient sites to correct growing season R_{eco} for air temperature at $25\,^{\circ}C$. The CO_2 flux was measured three times at the peak of the growing season (late

July) during 2006 and 2007 and the means of the three measurements were used for further analyses of GPP, R_{eco}, and NEE.

Spatial autocorrelation

Semivariograms were produced to evaluate spatial dependence and spatial autocorrelation of the variables measured at each grid within the plots at the three EML gradient sites. These variables include MT, soil temperature (T), soil moisture (VWC), TD within the active layer measured in July (TD), NDVI, and total aboveground biomass (B). We also produced semivariograms to evaluate spatial dependence and spatial autocorrelation of ecosystem carbon fluxes (R_{eco}, GPP, and NEE) at each grid point within the EML gradient sites.

Semivariance is a measure of dissimilarity, which therefore increases with increasing distance; if the semivariance curve is flat rather than increasing trend, this indicates insignificant spatial autocorrelation, or that the data are randomly distributed in space (Rossi *et al.*, 1992). Semivariance increases over distance because in nature dissimilarity tends to increase as the distance between sampled objects increases (Tobler, 1970). Beyond a certain distance called the range (*m*), the semivariance tends to flatten out, indicating that the variable is spatially independent beyond that distance range; at distances less than the range, the data are considered to be autocorrelated. The *y*-intercept from the model is called Nugget (C_0), which indicates the variability of closely spaced measurements and is often considered the sampling error. The *y*-value of where the semivariogram plateaus is called the Sill (*C*) and Spatial dependence (%) was calculated from the following equation (Jackson & Caldwell, 1993):

$$\text{Spatial dependence}\,(\%) = (C - C_0)/C \times 100. \quad (1)$$

Data for spatial autocorrelation were analyzed within each site. We chose a maximum distance in each analysis of 30 m and assigned each bin a 5 m width to insure an adequate number of samples in each bin. Therefore, in each semivariogram, there were at least 200 pairs of data points per distance interval. Semivariograms, ordinary block Kriging, and contour plots were generated with GS + VERSION 9.0 (Gamma Design Software, MI, USA) using the 10 nearest neighbors and a distance of 0.5 m between block centers.

Statistical analysis

Statistical analyses were conducted using SAS 9.0 (SAS Institute Inc., 2002) and R (R Development Core Team, 2005). We used Pearson's pairwise correlations to observe correlations between each pair of ecosystem variables. We constructed mixed effects models for GPP, R_{eco}, and NEE (response variables) using multiple ecosystem variables (MT, T, TD, VWC, NDVI, and B) measured at each grid within the EML gradient sites (explanatory variables) to find factors that significantly affect the response variables. The response variables were log-transformed to meet the assumptions of homoscedasticity and normally distributed residuals (Supporting Information,

Figure S1). This procedure was done using each EML site (Minimal, Moderate, and Extensive Thaw) as a 'block', as we knew *a priori* that spatial patterns by site were significantly different. By using only ecosystem variables that capture characteristics in different sites, we intended to construct a generalized model of carbon fluxes for tundra where thermokarst developed over the landscape, without being constrained by the location of previously defined EML gradient sites. From this analysis, the mixed-effects models are represented by

$$Y_k = \alpha_k \mathbf{X}_k + \varepsilon_k, \tag{2}$$

$$\varepsilon_k \sim \text{Normal}\,(0,\, \sigma_k^2 \Lambda_k), \tag{3}$$

where the subscript k indicates the response variable (i.e. $k = 1$, 2, 3 for GPP, R_{eco}, and NEE), $\mathbf{X}$ is the matrix of explanatory variables, α is the vector of parameters, ε is the residual error, and σ^2 is the variance term for the random effect and error terms (ε_k). To find the best fitting models for the response variables, we used a manual backward stepwise procedure with MT as a base variable, as we considered MT as the proxy of change in permafrost thaw and thermokarst development. In general, mixed effects models do not produce R^2; however, we generated R^2 using linear regression models to capture the predictive capability of the models. For this reason, we are presenting R^2 instead of adjusted R^2 in our results.

First, we constructed models without assuming any particular spatial autocorrelation pattern. Then, we included several different covariance models to account for spatial structure, as reflected by the covariance matrix, λ (Legendre *et al.*, 2002; Littell *et al.*, 2006). The spatial patterns observed in the semivariograms were used to explicitly declare the structure of the variance–covariance matrices in each model. We used Akaike's Information Criterion (AIC) to assess the adequacy of using these spatial variance-covariance structures in the model. We decided that the models were different 'substantially' if AIC values decreased by 2. The degrees of freedom in the models were adjusted with the Kenward–Rogers method to appropriately account for the spatial dependencies in the data. The model with the 'best-fit' was chosen as that model with the least number of variables which were relatively significant in the model. We used χ^2-test to show goodness-of-fit in measured and model predicted annual carbon fluxes.

Annual ecosystem carbon fluxes model from intensive measurements

We compared the effectiveness of ecosystem carbon flux models using ecosystem variables measured both extensively (50 grid points, few measurement dates) and intensively (six points, automated chamber semicontinuous measurements; Vogel *et al.*, 2009; Fig. 1) of ecosystem carbon fluxes (GPP, R_{eco}, and NEE). Vogel *et al.* (2009) established six replicate chamber collars at each of the three EML gradient sites and measured ecosystem carbon fluxes intensively throughout the growing season (May–September) from 2004 to 2006 using static chamber and automated chamber systems, simultaneously, to accurately estimate growing season carbon fluxes. Moreover, multiple measurements of R_{eco} were taken during the winter using a static chamber system and combined with the growing season in order to estimate annual carbon fluxes at the EML gradient sites.

Our goal was to determine whether the ecosystem carbon flux models we constructed from extensive measurements of growing season carbon fluxes were similar to those constructed with temporally intensive measurements of annual carbon fluxes. Growing season carbon fluxes are highly correlated to annual carbon fluxes, therefore, we assumed that the ecosystem variables that explained growing season carbon fluxes would also explain large variability in annual carbon fluxes. A mixed effects model was constructed using MT, TD, and B for intensive measurements of annual carbon fluxes. We then used the parameters estimated from intensive annual carbon flux models at the point scale to extrapolate annual carbon fluxes at the 50 grid points within the EML gradient sites.

MT was collected using the Theodolite Total Station surveying equipment and normalized with the same method used in this study. We used the 3-year mean (2004–2006) of TD measured at the peak of the growing season (mid-July) for this analysis. Aboveground biomass was estimated using point-framing method at the peak of the growing season in 2004.

Results

Spatial structures in surface subsidence at the EML gradient sites

As thermokarst develops, subsided areas become saturated with water, while elevated patches become drier. The EML gradient sites, previously defined as having different degrees of permafrost thaw and subsidence, showed different patterns of surface subsidence (Fig. 2) at each site. Minimal Thaw showed a weak spatial dependence (67.1%), or structural variance (see 'Spatial autocorrelation') and minimal variation in surface topography; Moderate Thaw showed a moderate spatial dependence (82.1%) and patchy distribution of surface subsidence; and Extensive Thaw showed the most spatial dependence (99.7%) with a more widespread surface subsidence throughout the survey area (Supporting Information Table S1).

Correlations and spatial patterns in ecosystem variables and ecosystem carbon fluxes

Across the EML gradient sites, MT was significantly correlated at $\alpha < 0.05$ level to four of the five measured ecosystem variables such as T (Pearson's correlation coefficient, $r = -0.2315$), VWC ($r = -0.4696$), TD ($r = -0.4887$), and NDVI ($r = -0.3070$; Table 1). Other ecosystem variables showed significant but moderate
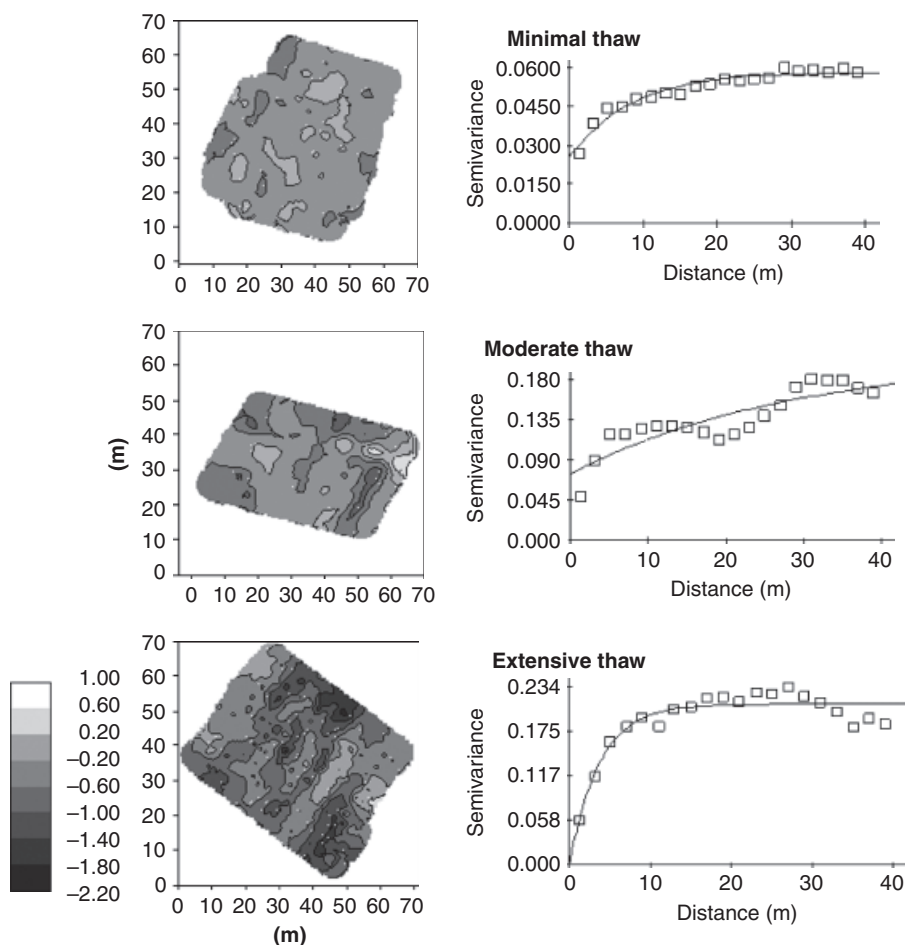
Fig. 2 The spatial patterns in surface subsidence (m) created by permafrost thaw and thermokarst. The values were generated by using semivariogram and ordinary Kriging. Negative values indicate subsided surface, whereas positive values indicate elevated or non-subsided surface.

Table 1 Pearson's pairwise correlation coefficients of the explanatory variables at the three EML gradient sites combined

	MT	T	VWC	TD	B	NDVI
MT		−0.2315	−0.4696	−0.4887	−0.0896	−0.3070
T	0.0067		0.0170	0.3911	0.2158	0.0295
VWC	0.0000	0.8362		0.3144	−0.0770	0.1297
TD	0.0000	0.0000	0.0001		0.0998	0.3003
B	0.2993	0.0080	0.3488	0.2244		0.1339
NDVI	0.0003	0.7213	0.1148	0.0002	0.1036	

The bolded values are correlation coefficients and the non-bolded values are *P*-values.
MT, surface subsidence measured by relative elevation noted as microtopography; T, soil temperature at 10 cm; VWC, volumetric water content at 10 cm; TD, soil thaw depth measured in late July; B, aboveground biomass measured by point-framing method; NDVI, normalized difference vegetation index; EML, Eight Mile Lake.

correlations with other variables: TD was correlated to T ($r = 0.3911$), VWC ($r = 0.3144$), and NDVI ($r = 0.3003$), and B was correlated to T ($r = 0.2158$). This indicates that surface subsidence created by permafrost thaw and thermokarst development is significantly related to soil environment and plant biomass, which are likely responding to this ground subsidence.

Within each plot, more ecosystem variables (MT, TD, VWC, NDVI) in the Extensive Thaw site showed spatial dependence (Table 2) and greater range of autocorrelation than those of Moderate (T and TD) and Minimal Thaw (TD and VWC). Semivariograms estimated for the remaining ecosystem variables (i.e. MT, T, NDVI, and B in Minimal Thaw) indicated a lack of significant autocorrelation (nugget only model), and these data were assumed to have random spatial distributions. There was no spatial structure shown in B at any of the three sites. On the other hand, NDVI showed moderate spatial dependence at Extensive Thaw (Spa-

Table 2 Model parameters of the curves fitted through each semivariogram in ecosystem variables

Site	Variable	Model	Nugget	Sill	Autocorrelation distance (m)	Spatial dependence (%)
Minimal Thaw	MT	LIN	0.00453	–	–	–
	T	LIN	1.668	–	–	–
	TD	GAU	13.203	23.814	2.9	44.6
	VWC	EXP	0.00132	0.005	–	73.5
	NDVI	LIN	0.00155	–	–	–
	B	LIN	26105.7	–	–	–
Moderate Thaw	MT	LIN	0.00614	–	–	–
	T	GAU	0.191	2.292	5.2	91.7
	TD	GAU	22.997	41.812	5.2	45.0
	VWC	LIN	0.00187	–	–	–
	NDVI	LIN	0.00728	–	–	–
	B	LIN	19144.8	–	–	–
Extensive Thaw	MT	EXP	0.00821	0.032	–	74.4
	T	EXP	1.562	2.357	3.5	33.7
	TD	GAU	86.427	127.500	4.3	32.2
	VWC	EXP	0.00164	0.003	39.6	50.2
	NDVI	EXP	0.00417	0.006	3.4	29.7
	B	LIN	17290.9	–	–	–

The nugget (C_0) is intercept of graph, sill (C) is semivariance of each graph where it plateaus, range is the distance where the plateau begins in meters, and spatial dependence [$(C-C_0)/C \times 100$] is the ratio of structural to population variance.
MT, surface subsidence measured by relative elevation noted as microtopography; T, soil temperature at 10 cm; TD, soil thaw depth measured in late July; VWC, volumetric water content at 10 cm; NDVI, normalized difference vegetation index; B, aboveground biomass measured by point-framing method; EXP, exponential; GAU, Gaussian; LIN, linear.

tial dependence = 29.7%), even though B and NDVI were significantly correlated to each other. Spatial dependence of the variables ranged widely, from 29.7% to 91.7%. It is important to note here that these analyses were performed on measurements made at 5 m grid spacings but the large majority of the observed microtopographic autocorrelation in Fig. 2 occurred at a scale of <5 m (Supporting Information Table S1).

Construction of extensive ecosystem carbon flux models

Summary statistics of extensive growing season carbon fluxes estimated from the 50 grid points within the EML gradient sites are provided in Supporting Information Table S2. Among the measured variables, MT, TD, and B best explained GPP (AIC = −164.5; $P = 0.2846$, $R^2 = 0.2573$), MT, TD, and B best explained R_{eco} (AIC = −97.0; p = 0.3892, $R^2 = 0.2158$), and MT and TD best explained NEE (AIC = −88.5; $P = 0.0132$, $R^2 = 0.1225$) (Table 3). We then added spatial covariance structure to the models to observe which spatial covariance structure enhances the models from the best fit models. For all three extensive ecosystem carbon flux models (R_{eco}, GPP, and NEE), adding exponential and power covariance structure to the best fit models resulted in the lowest AIC values (Table 4), but adding

exponential covariance structure slightly lowered P-values of explanatory variables in the models.

Annual ecosystem carbon flux models from intensive measurements

We used the three ecosystem variables (MT, TD, and B; Table 3) to extrapolate our growing season carbon fluxes to annual carbon fluxes (Table 5) using data collected intensively at six points within each of the EML gradient site by Vogel *et al.* (2009). In this intensive dataset, annual GPP was explained by MT, TD, and B ($P = 0.0217$, $R^2 = 0.7984$), annual R_{eco} was explained by MT, TD, and B ($P = 0.0322$, $R^2 = 0.7646$), and annual NEE was explained by MT, TD, and B ($P = 0.0642$, $R^2 = 0.2203$). Figure 3 shows 1 : 1 fit between measured and model predicted values of annual GPP, R_{eco}, and NEE derived from MT, TD, and B from the intensive measurements. The χ^2-values of measured and model predicted annual GPP, R_{eco}, and NEE were 3.59, 3.50, and 12.48, respectively ($F_{16, 0.05} = 26.30$). The goodness-of-fit test showed that measured and model predicted values of annual GPP, R_{eco}, and NEE were statistically not different. MT was not significant in any of the carbon flux models that included additional variables, which may be due to the strong correlation shown between MT and TD (Pearson's correlation coefficient,

Table 3 The carbon flux models constructed using measured ecosystem variables from the EML gradient sites combined

Carbon fluxes	Model	R^2	AIC	P-value	MT	TD	B
GPP	MT	0.1224	−146.1	0.5940	−0.5090 (<0.0001)	–	–
	MT + TD	0.2165	−159.9	0.4691	−0.2606 (0.0485)	0.6072 (0.0001)	–
	MT + B	0.1690	−150.7	0.4300	−0.4764 (0.0001)	–	0.2101 (0.0059)
	MT + TD + B	0.2573	−164.5	0.2846	−0.2348 (0.0664)	0.5858 (0.0001)	0.2014 (0.0055)
	MT + TD + B + *exp*	–	−168.3	0.0309	−0.1833 (0.1933)	0.5314 (0.0006)	0.1749 (0.0135)
R_{eco}	MT	0.0956	−82.7	0.3264	−0.5884 (0.0001)	–	–
	MT + TD	0.1439	−89.8	0.1749	−0.3486 (0.0348)	0.5425 (0.0041)	–
	MT + B	0.1729	−90.9	0.4910	−0.5420 (0.0003)	–	0.3196 (0.0011)
	MT + TD + B	0.2158	−97.0	0.3892	−0.3257 (0.0454)	0.5016 (0.0074)	0.3035 (0.0017)
	MT + TD + B + *exp*	–	−102.0	0.0244	−0.2443 (0.1272)	0.4624 (0.0091)	0.2394 (0.0082)
NEE	MT	0.0806	−84.2	0.0099	−0.4631 (0.0035)	–	–
	MT + TD	0.1225	−88.5	0.0132	−0.2839 (0.1001)	0.4779 (0.0202)	–
	MT + TD + *exp*	–	−94.6	0.0009	−0.1861 (0.3336)	0.5101 (0.0103)	–

Values in MT, TD, and B columns are parameter estimates and the values in parentheses are P-values of each variable in the model.
A log transformation of the response variables was used to meet the assumption of normally distributed data.
GPP, gross primary production; R_{eco}, ecosystem respiration; NEE, net ecosystem exchange of CO_2. MT, surface subsidence measured by relative elevation noted as microtopography; TD, soil thaw depth measured in late July; B, aboveground biomass measured by point-framing method; *exp*, exponential spatial covariance structure; EML, Eight Mile Lake.

Table 4 The AIC values of the growing season carbon flux models (GPP, R_{eco}, NEE) with and without spatial covariance structures

Spatial covariance structure	AIC values		
	GPP	R_{eco}	NEE
None	−164.5	−97.0	−88.5
Exponential	−168.4	−102.0	−94.6
Spherical	−153.5	−91.4	−73.5
Power	−168.4	−102.0	−94.6
Gaussian	−158.5	−91.0	−82.5
Anisotrophy	–	−92.6	–

AIC, Akaike's Information Criterion; GPP, gross primary production; R_{eco}, ecosystem respiration; NEE, net ecosystem exchange of CO_2.

$r = -0.8302$, $P < 0.0001$); however, MT was correlated to GPP, R_{eco}, and NEE by itself at $P = 0.0860$, 0.0592, and 0.1318, respectively, showing that it is still an important predictor of ecosystem carbon fluxes. The same group of variables that were significant predictors in the annual GPP and R_{eco} models constructed using extensive measurements was significant in these models (Table 3).

We then extrapolated annual carbon fluxes using MT, TD, and B from the six-point intensive annual carbon flux models (Table 6) to 50 grid point area within the EML gradient sites. Mean annual R_{eco} at Moderate and Extensive Thaw were significantly smaller (more negative value, more carbon release to the atmosphere) than at Minimal Thaw ($P = 0.0006$), though Extensive Thaw

was different from Moderate Thaw only at $P = 0.0812$. Mean annual GPP at Moderate and Extensive Thaw were significantly greater (more positive value, more carbon uptake to the ecosystem) than at Minimal Thaw ($P = 0.0043$), but mean annual GPP at Moderate and Extensive Thaw sites were not statistically different. Mean annual NEE at Moderate and Extensive Thaw were significantly greater (positive values represent carbon uptake to the ecosystem and negative values represent carbon release to the atmosphere) than at Minimal Thaw ($P = 0.0076$), but Moderate and Extensive Thaw were not statistically different. There was a significant difference ($P < 0.0001$) between modeled annual NEE estimated from the ecosystem variables, and annual NEE estimated from the difference between modeled annual R_{eco} and annual GPP. When annual NEE was estimated using the difference between annual R_{eco} and annual GPP, it was -30.1 ± 17.3, 8.1 ± 16.5, and $-6.0 \pm 14.1 \, g \, CO_2$–$C \, m^{-2}$ at Minimal, Moderate, and Extensive Thaw, respectively. This may be due to the low explanatory power of the annual NEE model (Table 5), which is typical for NEE measurements, the difference of two large offsetting fluxes.

The Kriging maps of predicted annual GPP and R_{eco} for the 50 grid points at the three EML gradient sites showed spatial patterns on a landscape undergoing permafrost thaw and thermokarst development (Fig. 4). There was stronger spatial pattern shown in GPP of Moderate Thaw site and R_{eco} at Extensive Thaw site. Minimal Thaw did not show substantial spatial pattern in GPP nor R_{eco}. The spatial patterns shown in the extrapolated annual GPP and R_{eco} for the 50 grid

Table 5 Annual carbon flux models using same group of ecosystem variables chosen from the plot scale carbon flux models

Carbon fluxes	Model	R^2	AIC	P-value	MT	TD	B
Annual GPP	MT	0.5030	179.2	0.0592	0.0005	–	–
	TD + B	0.8011	158.0	0.0161	–	0.0484	0.0028
	MT + TD + B	0.7984	140.3	0.0217	0.7300	0.1154	0.0279
Annual R_{eco}	MT	0.4505	170.2	0.0860	0.0051	–	–
	MT + TD	0.7051	146.0	0.0260	0.8782	0.0123	–
	MT + TD + B	0.7646	131.5	0.0322	0.7226	0.0790	0.1783
Annual NEE	MT	0.1447	163.6	0.1318	0.9873	–	–
	MT + TD	0.1479	148.9	0.0175	0.1752	0.0882	–
	MT + TD + B	0.2203	135.4	0.0642	0.0548	0.0254	0.1261

The P-value column represents P-value of the whole model. MT, T, TD, and B columns represent p-value of the variables in the model.
GPP, gross primary production; R_{eco}, ecosystem respiration; NEE, net ecosystem exchange of CO_2; MT, surface subsidence measured by relative elevation noted as microtopography; TD, soil thaw depth measured in late July; T, mean growing season soil temperature monitored from 2004 to 2007 at 10 cm; B, aboveground biomass measured by point-framing method.
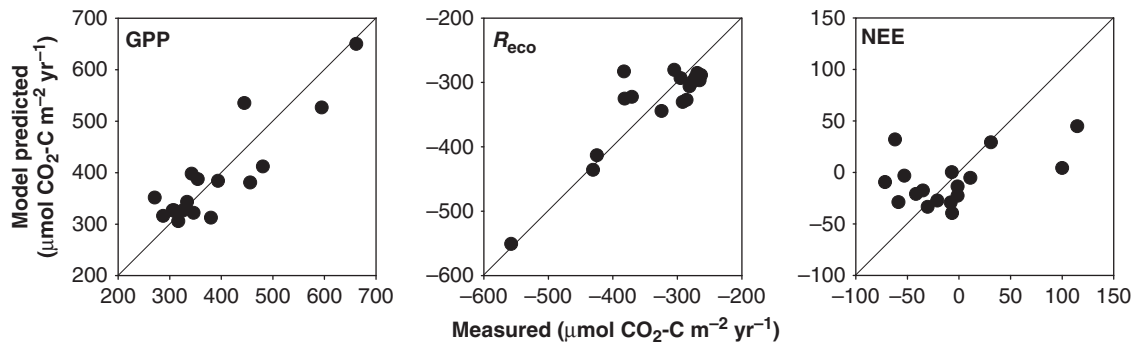

Fig. 3 A 1:1 fit between measured and model predicted values of annual GPP, R_{eco}, and NEE from intensive measurements of ecosystem fluxes ($n = 17$) at the Eight Mile Lake (EML) gradient sites. Each ecosystem carbon flux model was produced using surface subsidence (MT), seasonal thaw depth (TD), and aboveground plant biomass (B). The goodness-of-fit test for annual GPP, R_{eco}, and NEE showed that measured and model predicted values were statistically not different. GPP, gross primary production; R_{eco}, ecosystem respiration; NEE, net ecosystem exchange of CO_2.

points were similar to the pattern shown from MT (Fig. 2) at the EML gradient sites.

Discussion

Many ecosystem carbon flux studies have been performed either on a point scale using the static or automated chamber methods, or on a much larger scale using the eddy covariance or remote sensing methods. To estimate carbon fluxes in changing ecosystems, it is important to capture the underlying principles of the spatial variability of the fluxes. This can only be attained by a large-scale approach; however, it takes extensive amount of resources to make observations at both a large scale and with the detailed temporal coverage that is generally obtained by a point scale method. On the other hand, eddy covariance or remote sensing

methods cannot depict fine scale spatial variation. Similar to ecosystem carbon flux measurements, modeling ecosystem carbon fluxes that includes precision and accuracy represented as intensive and extensive measurements of ecosystem carbon fluxes. In this study, we attempted to show the balance between intensive and extensive measurements of ecosystem carbon fluxes and modeling these at a landscape scale.

In order to effectively extrapolate our point measurements of ecosystem carbon fluxes within the landscape, we needed to account for the observed spatial patterns shown in ecosystem variables. The spatial pattern in surface subsidence was distinct for each of the three EML gradient sites that corresponded to different degrees of permafrost thaw and thermokarst development (Fig. 2 and Supporting Information Table S1). The Extensive Thaw site had the greatest number of

variables containing spatial patterns, indicating that changes in soil environment are correlated with the degree of permafrost thaw and thermokarst development, which supported the assumption that permafrost thaw and thermokarst development both influenced the soil environment (Table 1). When thermokarst develops, subsided areas are more likely to collect snow in the winter (Osterkamp *et al.*, 2000; Jorgenson *et al.*, 2006). As a result, the snow insulates the soil and keeps the area warmer during the winter leaving the areas exposed colder in the winter as wind redistributes snow across the landscape (Osterkamp, 2007; Osterkamp *et al.*, 2009). Furthermore, during the

summer, warm winter soil has positive feedback on soil temperatures (Stieglitz *et al.*, 2003). Warm soil temperatures may stimulate microbial decomposition of soil organic matter and release more nutrients back to soil, which may stimulate primary production in localized spots via increased shrub growth (Shaver *et al.*, 2001; Schuur *et al.*, 2007). Therefore, surface subsidence created as a result of permafrost thaw and thermokarst development alters ecosystem properties and can positively feed back to more permafrost thaw as a result.

Changes in ecosystem properties created as a result of permafrost thaw and thermokarst development then affects ecosystem carbon cycling via altering carbon uptake represented as plant photosynthesis and carbon emissions represented as decomposition of organic matter and plant respiration. Our extensive growing season carbon flux models (Table 3) showed that patterns in growing season carbon fluxes in upland tundra were described by three ecosystem variables: surface subsidence (MT), seasonal TD in the active layer, and aboveground plant biomass (B). Notably, all of these ecosystem variables had spatial structure across the landscape created as a result of permafrost thaw and thermokarst development; this variation needed to be taken into account for the models to become significant (Table 3). As shown in our mixed effects models, using

Table 6 Mean annual GPP, R_{eco}, and NEE in $g\,CO_2$–$C\,m^{-2}$ (Mean $\pm$ SE) for the EML gradient sites estimated over a larger scale in space using parameters estimated from the annual carbon flux models

	Minimal Thaw	Moderate Thaw	Extensive Thaw
Annual GPP	349.4 ± 17.7	421.5 ± 17.0	426.4 ± 17.7
Annual R_{eco}	-379.5 ± 5.7	-413.5 ± 7.6	-432.4 ± 11.1
Annual NEE	-43.4 ± 11.8	0.1 ± 10.6	-8.8 ± 8.7

EML, Eight Mile Lake; GPP, gross primary production; R_{eco}, ecosystem respiration; NEE, net ecosystem exchange of CO_2.
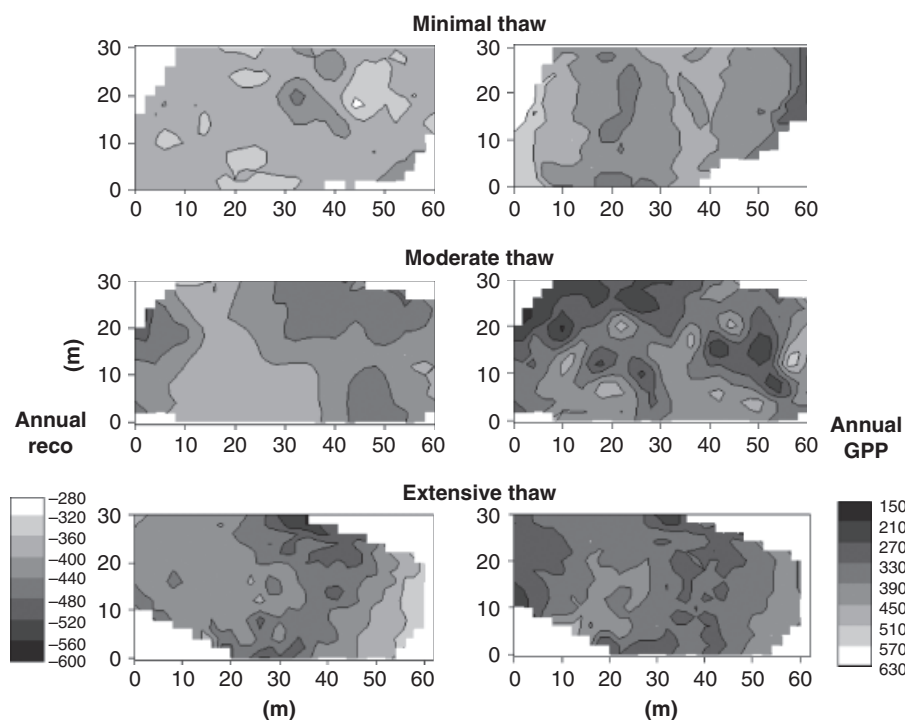

Fig. 4 The spatial patterns in predicted annual R_{eco} and GPP ($g\,CO_2$–$C\,m^{-2}$) at the three Eight Mile Lake (EML) gradient sites using ordinary Kriging. Left panels are R_{eco} and right panels are GPP. Negative values indicate CO_2 emissions, and positive values indicate CO_2 uptake from atmosphere to the ecosystem. GPP, gross primary production; R_{eco}, ecosystem respiration; NEE, net ecosystem exchange of CO_2.

spatial covariance structure in the models does explain part of the variance (decreased AIC values more than 2), but did not significantly enhance the model fit via increased R^2 due to the nature of mixed models. (Refer to 'Materials and methods' section that mixed models do not produce R^2.) Nevertheless, using spatial structure in ecosystem carbon flux models captured some of the variability found at the larger scale (Table 3). In particular, explaining changes in carbon balance across tundra ecosystems that are thawing appears to require fine scale (<5 m) measurements in order to extrapolate across the unmeasured part of the landscape.

Previous studies have explained ecosystem carbon fluxes using ecosystem measurements in tundra that are known drivers of biological processes. For example, ecosystem researchers have observed increased GPP as a function of increased soil temperature (Starr *et al.*, 2004; Oberbauer *et al.*, 2007), increased R_{eco} as a function of increased soil temperature (Shaver *et al.*, 1992; Chapin *et al.*, 2000; Oechel *et al.*, 2000), and increased R_{eco} as a function of increased soil moisture (Chapin *et al.*, 1988; Oberbauer *et al.*, 1992; Illeris *et al.*, 2004). Others have also observed increased GPP and R_{eco} as a function of increased NDVI (Boelman *et al.*, 2003; La Puma *et al.*, 2007) or LAI derived from NDVI (Shaver *et al.*, 2007), differences in GPP and R_{eco} as a function of different vegetation types (Sullivan *et al.*, 2008), and increased NEE as a function of increased ALT (Weller *et al.*, 1995). In this study, we showed the relationship between ecosystem carbon fluxes and previously identified variables, and have also identified proxy variables specific to permafrost landscape (i.e. surface subsidence and TD) to describe long-term carbon fluxes under permafrost thaw. Indeed, these ecosystem variables, along with aboveground biomass, are better predictors of long-term carbon fluxes at this site than are other ecosystem variables such as soil moisture. This does not imply that the excluded variables are unimportant in explaining ecosystem carbon fluxes. Rather, it highlights the significant correlations that exist between the omitted variables and the variables included in the model (Table 1), and suggests that a static variable such as surface subsidence and TD can represent redistribution of ecosystem factors such as soil moisture and temperature in regions where thermokarst has developed.

Among the ecosystem measurements that explained ecosystem carbon fluxes in our study, surface subsidence maybe the most notable. Topographic patterns created by permafrost thaw and thermokarst development may not have a direct effect on ecosystem carbon fluxes; instead have an indirect effect due to factors such as changes in soil moisture or vegetation driven by topographic patterns. The relationships between topo-graphic patterns and carbon emissions have been shown in various ecosystems (Hanson *et al.*, 1993; Kang *et al.*, 2003; Epron *et al.*, 2006; Sommerkorn, 2008; Martin & Bolstad, 2009), but most of which concluded that changes in topographic features indirectly affect soil environment (i.e. soil temperature, moisture, bulk density, root density) and influenced ecosystem carbon fluxes as a result. In addition, Riveros-Iregui & McGlynn (2009) have shown that different patterns of slope in the topography changed patterns of watershed and soil moisture, which in turn affected ecosystem carbon fluxes. These results support that topographic patterns are useful predictors of ecosystem carbon fluxes because they often represent larger scale in the landscape covering the entire watershed area (Riveros-Iregui & McGlynn, 2009). Our results imply that ecosystem carbon fluxes are affected by surface subsidence created by permafrost thaw and thermokarst development not through a direct effect, but indirectly as surface subsidence stimulates changes in ecosystem processes.

The number of measurements needed to accurately represent natural phenomena has always been a question for scientists because it takes much resources and time to make observations at both a large scale and with the detailed temporal coverage. In previous research (Lee *et al.*, 2010), we showed that 33% of the variability in soil CO_2 production was explained by MT (including other ecosystem variables, an adjusted $R^2 = 0.48$ was obtained), which indicates the power of repeated measurements in explaining the variability of ecosystem carbon fluxes. If the variables were measured repeatedly throughout the growing season over several years, the model R^2-value would have been higher than the current estimates as demonstrated by the intensive site analysis. Therefore, our results are valuable as is because our results not only show the extent of spatial variability in carbon fluxes, but also show that the variability can be reduced by multiple measurements of carbon fluxes over time.

Our extensive models may show low R^2 ($R^2 < 0.30$), but our intensive models show high R^2 ($R^2 > 0.90$), which is a direct example of how statistically R^2 changes when there are spatially extensive measurements (R^2 decreases) and temporally extensive measurements (R^2 increases). A recent research conducted in tundra sites at the north slope of Alaska and Sweden demonstrated that GPP, R_{eco}, and NEE could be modeled using base R_{eco} measurements, PAR, soil temperature, and leaf area index with R^2 values ranging from 0.62 to 0.98 in tundra ecosystems regardless of the vegetation type (Shaver *et al.*, 2007). Indeed, the R^2 values of our extensive ecosystem carbon flux models were much lower compared with those derived from

Shaver et al. (2007). This was because our ecosystem carbon flux models were derived from measured static ecosystem variables alone, whereas, Shaver et al. (2007) used base respiration (a model fitted value) to estimate ecosystem carbon balance. Moreover, the range of their measurements was much greater than our measurement range (i.e. NEE in our study ranged from -8 to $0\,\mu\mathrm{mol\,CO_2\,m^{-2}\,s^{-1}}$, whereas NEE in Shaver et al. (2007) ranged from -15 to $8\,\mu\mathrm{mol\,CO_2\,m^{-2}\,s^{-1}}$, three-fold greater than our measurement range) because they took measurements from various tundra sites with very different vegetation types, which may be one of the factors in higher R^2 during statistical analysis.

The intensive ecosystem carbon flux models presented in this study show that surface subsidence created by permafrost thaw and thermokarst development, seasonal TD, and aboveground biomass were better predictors in extrapolating ecosystem carbon fluxes than other ecosystem variables (Table 4). A similar approach was used to model CO_2 and CH_4 emissions in tundra ecosystem using soil temperature and water table depth (Bubier et al., 1993; Heikkinen et al., 2002), and driving variables that have been verified through the use of gravity spaceborne data (Anthony Bloom et al., 2010). Additionally, several studies used point measurements inside the eddy covariance tower footprint or satellite image to verify the scaling (Oechel et al., 2000; Riveros-Iregui et al., 2008). The relatively high R^2 in our intensive models show that the environmental variables we used best captures long term carbon flux that is of interest rather than short term variability. Indeed, we observed that the measured annual carbon fluxes and model predicted annual carbon fluxes were statistically not different (Fig. 3), giving us confidence that this may also be extrapolated to a larger tundra landscape where permafrost is thawing (Fig. 4).

The spatial patterns in predicted ecosystem carbon fluxes in the 50 grid points within the EML gradient sites (Fig. 4) were consistent with the trends in ecosystem carbon fluxes in previous studies using intensive point scale measurements (Schuur et al., 2009; Vogel et al., 2009). After intensively measuring carbon fluxes at the EML gradient sites, Vogel et al. (2009) showed that GPP and R_{eco} increased as permafrost thaw progressed, but greater increase in R_{eco} at the Extensive Thaw site made it a carbon source, when Moderate Thaw site was a carbon sink. The Kriging map of annual carbon fluxes in plot scale (Fig. 4) indicated the lowest spatial variability present in annual GPP and annual R_{eco} at Minimal Thaw. However, there was higher variability in annual GPP in Moderate Thaw and in annual R_{eco} in Extensive Thaw.

In summary, we showed that static ecosystem variables that do not change on daily basis (i.e. surface subsidence created by thermokarst development, seasonal TD in the active layer, and aboveground biomass) can be extrapolated as proxy variables to explain long-term ecosystem carbon fluxes in upland tundra where permafrost is thawing. These same variables did not predict nearly as well short-term variation in carbon fluxes, likely because they were integrative variables that changed very slowly during the growing season. Moreover, this study shows the possibilities of scaling measurements from a small spatial scale and successfully extrapolating to a larger area. However, using spatial structure to determine changes in variables across the landscape is best with more tightly clustered measurements. Most of the spatial dependence occurred at scales of $<5\,\mathrm{m}$ that we detected mainly with our original ground subsidence survey rather than the $50\,\mathrm{m}$ grid. This approach of using slowly changing relatively static variable as proxy for long-term carbon fluxes may be useful for extrapolating to larger scales using remote sensing, aerial photography, or satellite imagery.

Acknowledgements

References

ACIA (2005) Arctic Climate Impact Assessment – Scientific Report. Cambridge University Press, New York, NY.

Anthony Bloom A, Palmer PI, Fraser A, Reay DS, Frankenberg C (2010) Large-scale controls of methanogenesis inferred from methane and gravity spaceborne data. Science, 327, 322–325.

Boelman NT, Stieglitz M, Griffin KL, Shaver GR (2005) Inter-annual variability of NDVI in response to long-term warming and fertilization in wet sedge and tussock tundra. Oecologia, 143, 588–597.

Boelman NT, Stieglitz M, Rueth HM, Sommerkorn M, Griffin KL, Shaver GR, Gamon JA (2003) Response of NDVI, biomass, and ecosystem gas exchange to long-term warming and fertilization in wet sedge tundra. Oecologia, 135, 414–421.

Bubier J, Costello A, Moore TR, Roulet NT, Savage K (1993) Microtopography and methane flux in Boreal Peatlands, Northern Ontario, Canada. Canadian Journal of Botany-Revue Canadienne De Botanique, 71, 1056–1063.

Bubier JL, Bhatia G, Moore TR, Roulet NT, Lafleur PM (2003) Spatial and temporal variability in growing-season net ecosystem carbon dioxide exchange at a large peatland in Ontario, Canada. Ecosystems, 6, 353–367.

Chapin FS, Fetcher N, Kielland K, Everett KR, Linkins AE (1988) Productivity and nutrient cycling of Alaskan Tundra – enhancement by flowing soil-water. Ecology, 69, 693–702.

Chapin FS, McGuire AD, Randerson J *et al.* (2000) Arctic and boreal ecosystems of western North America as components of the climate system. *Global Change Biology*, **6**, 211–223.

Davis TN (2001) *Permafrost: A Guide to Frozen Ground in Transition*. University of Alaska Press, Fairbanks, AL.

Epron D, Bosc A, Bonal D, Freycon V (2006) Spatial variation of soil respiration across a topographic gradient in a tropical rain forest in French Guiana. *Journal of Tropical Ecology*, **22**, 565–574.

Hanson PJ, Wullschleger SD, Bohlman SA, Todd DE (1993) Seasonal and topographic patterns of forest floor CO_2 efflux from an upland Oak forest. *Tree Physiology*, **13**, 1–15.

Harvey LDD (2000) Upscaling in global change research. *Climatic Change*, **44**, 225–263.

Heikkinen JEP, Elsakov V, Martikainen PJ (2002) Carbon dioxide and methane dynamics and annual carbon balance in tundra wetland in NE Europe, Russia. *Global Biogeochemical Cycles*, **16**, 1115, doi: 10.1029/2002GB001930.

Hinzman LD, Bettez ND, Bolton WR *et al.* (2005) Evidence and implications of recent climate change in northern Alaska and other arctic regions. *Climatic Change*, **72**, 251–298.

Illeris L, Konig SM, Grogan P, Jonasson S, Michelsen A, Ro-Poulsen H (2004) Growing-season carbon dioxide flux in a dry subarctic heath: responses to long-term manipulations. *Arctic, Antarctic and Alpine Research*, **36**, 456–463.

IPCC (2007) *Climate Change 2007: The Physical Science Basis*. Cambridge University Press, Cambridge, UK.

Jackson RB, Caldwell MM (1993) Geostatistical patterns of soil heterogeneity around individual perennial plants. *Journal of Ecology*, **81**, 683–692.

Jorgenson MT, Shur YL, Pullman ER (2006) Abrupt increase in permafrost degradation in Arctic Alaska. *Geophysical Research Letters*, **33**, L02503, doi: 10.1029/2005GL024960.

Kang SY, Doh S, Lee D, Jin VL, Kimball JS (2003) Topographic and climatic controls on soil respiration in six temperate mixed-hardwood forest slopes, Korea. *Global Change Biology*, **9**, 1427–1437.

Kwon HJ, Oechel WC, Zulueta RC, Hastings SJ (2006) Effects of climate variability on carbon sequestration among adjacent wet sedge tundra and moist tussock tundra ecosystems. *Journal of Geophysical Research-Biogeosciences*, **111**, G03014, doi: 10.1029/2005JG000036.

La Puma IP, Philippi TE, Oberbauer SF (2007) Relating NDVI to ecosystem CO_2 exchange patterns in response to season length and soil warming manipulations in arctic Alaska. *Remote Sensing of Environment*, **109**, 225–236.

Lee H, Schuur EAG, Vogel JG (2007) Spatial variation in carbon release from Arctic Tundra resulting from microtopography created by permafrost thawing. *EOS Transactions American Geophysical Union*, **88**, Fall Meet. Suppl, Abstract B23D-1602.

Lee H, Schuur EAG, Vogel JG (2010) Soil CO_2 production in upland tundra where permafrost is thawing. *Journal of Geophysical Research-Biogeosciences*, **115**, G01009, doi: 10.1029/2008JG000906.

Legendre P, Dale MRT, Fortin MJ, Gurevitch J, Hohn M, Myers D (2002) The consequences of spatial structure for the design and analysis of ecological field surveys. *Ecography*, **25**, 601–615.

Littell RC, Milliken GA, Stroup WW, Wolfinger RD, Shabenberger O (2006) *SAS for Mixed Models*. SAS Institute Inc., Cary, NC, USA.

Little JD, Sandall H, Walegur MT, Nelson FE (2003) Application of differential global positioning systems to monitor frost heave and thaw settlement in tundra environments. *Permafrost and Periglacial Processes*, **14**, 349–357.

Macdonald GM, Edwards TWD, Moser KA, Pienitz R, Smol JP (1993) Rapid response of treeline vegetation and lakes to past climate warming. *Nature*, **361**, 243–246.

Mack MC, Schuur EAG, Bret-Harte MS, Shaver GR, Chapin FS (2004) Ecosystem carbon storage in arctic tundra reduced by long-term nutrient fertilization. *Nature*, **431**, 440–443.

Martin JG, Bolstad PV (2009) Variation of soil respiration at three spatial scales: components within measurements, intra-site variation and patterns on the landscape. *Soil Biology and Biochemistry*, **41**, 530–543.

Oberbauer SF, Gillespie CT, Cheng W, Gebauer R, Serra AS, Tenhunen JD (1992) Environmental-effects on CO_2 efflux from Riparian tundra in the Northern Foothills of the Brooks Range, Alaska, USA. *Oecologia*, **92**, 568–577.

Oberbauer SF, Tweedie CE, Welker JM *et al.* (2007) Tundra CO_2 fluxes in response to experimental warming across latitudinal and moisture gradients. *Ecological Monographs*, **77**, 221–238.

Oechel WC, Vourlitis GL, Hastings SJ, Zulueta RC, Hinzman L, Kane D (2000) Acclimation of ecosystem CO_2 exchange in the Alaskan Arctic in response to decadal climate warming. *Nature*, **406**, 978–981.

Osterkamp TE (2007) Causes of warming and thawing permafrost in Alaska. *EOS, Transactions American Geophysical Union*, **88**, 522.

Osterkamp TE, Jorgenson MT, Schuur EAG, Shur YL, Kanevskiy MZ, Vogel JG, Tumskoy VE (2009) Physical and ecological changes associated with warming permafrost and thermokarst in interior Alaska. *Permafrost and Periglacial Processes*, **20**, 235–256.

Osterkamp TE, Romanovsky VE (1999) Evidence for warming and thawing of discontinuous permafrost in Alaska. *Permafrost and Periglacial Processes*, **10**, 17–37.

Osterkamp TE, Viereck L, Shur Y, Jorgenson MT, Racine C, Doyle A, Boone RD (2000) Observations of thermokarst and its impact on boreal forests in Alaska, USA. *Arctic, Antarctic and Alpine Research*, **32**, 303–315.

Overpeck J, Hughen K, Hardy D *et al.* (1997) Arctic environmental change of the last four centuries. *Science*, **278**, 1251–1256.

Riveros-Iregui DA, McGlynn BL (2009) Landscape structure control on soil CO_2 efflux variability in complex terrain: scaling from point observations to watershed scale fluxes. *Journal of Geophysical Research-Biogeosciences*, **114**, G02010, doi: 10.1029/2008jg000885.

Riveros-Iregui DA, McGlynn BL, Epstein HE, Welsch DL (2008) Interpretation and evaluation of combined measurement techniques for soil CO_2 efflux: discrete surface chambers and continuous soil CO_2 concentration probes. *Journal of Geophysical Research-Biogeosciences*, **113**, G04027, doi: 10.1029/2008JG000811.

Rossi RE, Mulla DJ, Journel AG, Franz EH (1992) Geostatistical tools for modeling and interpreting ecological spatial dependence. *Ecological Monographs*, **62**, 277–314.

Schuur EAG, Bockheim J, Canadell JG *et al.* (2008) Vulnerability of permafrost carbon to climate change: implications for the global carbon cycle. *Bioscience*, **58**, 701–714.

Schuur EAG, Crummer KG, Vogel JG, Mack MC (2007) Plant species composition and productivity following permafrost thaw and thermokarst in Alaskan tundra. *Ecosystems*, **10**, 280–292.

Schuur EAG, Vogel JG, Crummer KG, Lee H, Sickman JO, Osterkamp TE (2009) The effect of permafrost thaw on old carbon release and net carbon exchange from tundra. *Nature*, **459**, 556–559.

Serreze MC, Walsh JE, Chapin FS *et al.* (2000) Observational evidence of recent change in the northern high-latitude environment. *Climatic Change*, **46**, 159–207.

Shaver GR, Billings WD, Chapin FS, Giblin AE, Nadelhoffer KJ, Oechel WC, Rastetter EB (1992) Global change and the carbon balance of Arctic ecosystems. *Bioscience*, **42**, 433–441.

Shaver GR, Bret-Harte SM, Jones MH, Johnstone J, Gough L, Laundre J, Chapin FS (2001) Species composition interacts with fertilizer to control long-term change in tundra productivity. *Ecology*, **82**, 3163–3181.

Shaver GR, Canadell J, Chapin FS *et al.* (2000) Global warming and terrestrial ecosystems: a conceptual framework for analysis. *Bioscience*, **50**, 871–882.

Shaver GR, Street LE, Rastetter EB, Van Wijk MT, Williams M (2007) Functional convergence in regulation of net CO_2 flux in heterogeneous tundra landscapes in Alaska and Sweden. *Journal of Ecology*, **95**, 802–817.

Sommerkorn M (2008) Micro-topographic patterns unravel controls of soil water and temperature on soil respiration in three Siberian tundra systems. *Soil Biology and Biochemistry*, **40**, 1792–1802.

Starr G, Neuman DS, Oberbauer SF (2004) Ecophysiological analysis of two arctic sedges under reduced root temperatures. *Physiologia Plantarum*, **120**, 458–464.

Stieglitz M, Dery SJ, Romanovsky VE, Osterkamp TE (2003) The role of snow cover in the warming of arctic permafrost. *Geophysical Research Letters*, **30**, 1721, doi: 10.1029/2003GL017337.

Sturm M, Schimel J, Michaelson G *et al.* (2005) Winter biological processes could help convert arctic tundra to shrubland. *Bioscience*, **55**, 17–26.

Sullivan PF, Arens SJT, Chimner RA, Welker JM (2008) Temperature and microtopography interact to control carbon cycling in a high arctic fen. *Ecosystems*, **11**, 61–76.

Tarnocai C, Canadell JG, Schuur EAG, Kuhry P, Mazhitova G, Zimov S (2009) Soil organic carbon pools in the northern circumpolar permafrost region. *Global Biogeochemical Cycles*, **23**, GB2023, doi: 10.1029/2008GB003327.

Thorney JHM, Johnson IR (1990) *Plant and Crop Modeling: A Mathematical Approach to Plant and Crop Physiology*. Clarendon Press, Oxford, UK.

Tobler WR (1970) Computer movie simulating urban growth in Detroit region. *Economic Geography*, **46**, 234–240.

Vogel JG, Schuur EAG, Trucco C, Lee H (2009) The carbon cycling response of tussock tundra to permafrost thaw and thermokarst development. *Journal of Geophysical Research-Biogeosciences*, **114**, G4, doi: 10.1029/2008JG000901.

Weller G, Chapin FS, Everett KR *et al.* (1995) The arctic flux study: a regional view of trace gas release. *Journal of Biogeography*, **22**, 365–374.

Williams M, Bell R, Spadavecchia L, Street LE, Van Wijk MT (2008) Upscaling leaf area index in an Arctic landscape through multiscale observations. *Global Change Biology*, **14**, 1517–1530.

Supporting Information

Additional Supporting Information may be found in the online version of this article:

Figure S1. Summary of response variable (GPP, Reco, and NEE) distribution. The response variables were log-transformed and normal distribution curve was fit.
Table S1. Model parameters of the sources fitted through each semivariogram in surface subsidence (MT) measured each site in 2005 shown in Figure 2. The sampling area was approximately 50 m × 50 m and 600 ± 50 points were sampled.
Table S2. Summary statistics of the explanatory variables used in the growing season carbon flux models for the three EML gradient sites.

Please note: Wiley-Blackwell are not responsible for the content or functionality of any supporting materials supplied by the authors. Any queries (other than missing material) should be directed to the corresponding author for the article.